行政院國家科學委員會補助專題研究計畫 ■ 成 果 報 告
□期中進度報告

（計畫名稱）

Synthesis, characterization and theoretical prediction of environmentally benign(AA')(BB')O3 multifunctional ferroelectric materials (A,A'=Na,K,Li, Bi,Ba,Sr;B,B'= Nb, Fe, Ti)

計畫類別：■ 個別型計畫 □ 整合型計畫
計畫編號：NSC97－2923－M－029 －001－MY3
執行期間：98 年8 月1 日至101 年7 月31 日

計畫主持人：程海東
共同主持人：曾俊元、周振嘉
計畫參與人員： 陳炳宜、馮奎智

成果報告類型(依經費核定清單規定繳交)：□精簡報告■完整報告

本成果報告包括以下應繳交之附件：
□赴國外出差或研習心得報告一份
□赴大陸地區出差或研習心得報告一份
□出席國際學術會議心得報告及發表之論文各一份
□國際合作研究計畫國外研究報告書一份

處理方式：除產學合作研究計畫、提升產業技術及人才培育研究計畫、列管計畫及下列情形者外，得立即公開查詢
□涉及專利或其他智慧財產權，□一年□二年後可公開查詢

執行單位：東海大學物理系

中 華 民 國 一0一年 七 月 三十一 日

Publications:

1. Comparative study between conventional and microwave sintered lead-free BNKT ceramics, Pin-Yi Chen, M B Suresh, Kun-Lin Lin, Chen-Chia Chou, Tseung-Yuen Tseng and Haydn H. D. Chen , Ferroelectrics, 381：1-5, 2009
2. Impedance Spectroscopic Study on the Effect of Defects with Li Doped BNKT Piezoelectric Ceramics, Pin-Yi Chen, M B Suresh, Kun-Lin Lin, Chen-Chia Chou, Tseung-Yuen Tseng and Haydn H. D. Chen, Ferroelectrics, 381: 100-104, 2009.
3. Correlation of Microstructures and Conductivities of Ferroelectric Ceramics Using Complex Impedance Spectroscopy, Pin-Yi Chen, Chen-Chia Chou, Tseung-Yuen Tseng and Haydn Chen, Japanese Journal of Applied Physics, 49: 061505, 2010.
4. Second Phase and Defect Formation in Bi0:5Na0:5_xKxTiO3 Ceramics, Pin-Yi Chen, Chen-Chia Chou, Tseung-Yuen Tseng and Haydn Chen, Japanese Journal of Applied Physics, 49: 061506, 2010.
5. Kuei Chih Feng, Chen Chia Chou, Li-Wen Chu and Haydn Chen, Influence of microstructures on variation of dielectric properties of ZrO_2 modified-$CaMgSi_2O_6$ diopside glass-ceramic under second thermal treatment, Ferroelectrics, 2011 accepted.
6. Kuei-Chih Feng, Chen-Chia Chou, Li-Wen Chu and Haydn Chen, Zirconia nucleating agent on microstructural and electrical properties of a $CaMgSi_2O_6$ diopside glass-ceramic for microwave dielectrics, Materials Research Bulletin, 47: 2851-2855, 2012.
7. Kuei-Chih Feng, Chen-Chia Chou, Cheng-Sao Chen, Li-Wen Chu and Haydn Chen, Phase Evolution and Electrical properties of copper-electroded $BaTi_4O_9$ Materials with BZBS glass system in reducing atmosphere, Ceramics International, 2012 accepted.
8. Pin-Yi Chen, Chen-Chia Chou, Cheng Nan Chen, Cheng-Sao Chen and Haydn Chen, The effects of aliovalent cations doping on electricfield-induced strain and microstructures of $(Bi_{0.5}\text{-}Na_{0.5})_{0.94}Ba_{0.06}TiO_3$ lead-free piezoceramics, Ceramics International, 2012 accepted.
9. Cheng-Sao Chen, Chen-Chia Chou, Yung-Shun Lin, Pin-Yi Chen and Haydn Chen, Effects of $CaTiO_3$ addition on microstructures and electrical properties of $Na_{0.52}K_{0.48}NbO_3$ lead-free piezoelectric ceramics, Ceramics International, 2012 accepted.

Second Phase and Defect Formation in $Bi_{0:5}Na_{0:5\_x}KxTiO_3$ Ceramics

Abstract

The second phase and defect formation mechanisms of [Bi0:5(Na1_xKx)0:5]TiO3 (BNKT100x) ceramics were investigated using electron microscopy, X-ray photoelectron spectroscopy (XPS), and electrical properties measurement. Experimental results indicated that second phase formation induces Bi-rich regions and compositional inhomogeneity within the matrix owing to the thermodynamic stability of potassium titanate. The Ti valence transition for BNKT ceramics sintered in air might be ascribed to the formation of secondary phase and low oxygen atmosphere, rather than simply attributed to the volatilization of bismuth. Li substitution at the A-site in BNKT ceramics suppresses formation of the second phase and Ti valence transition. Appropriate atmosphere control during material processing, such as sintering at higher oxygen pressure, and post oxidization annealing suppress oxygen vacancies and titanium valence transition, and therefore decrease the leakage current as well as improve electrical properties. # 2010 The Japan Society of Applied Physics.

1. Introduction

In recent years, lead-based $Pb(ZrTi)O_3$ materials have been restricted to use by legislation in some countries, because the toxicity of lead oxide and its high vapor pressure during processing jeopardize human's health and pollute the environment. Therefore, lead-free piezoelectric materials have attracted considerable attention worldwide as new materials in replacement of PZT-based piezoelectric ceramics.

Lead-free piezoelectric materials with perovskite structure, such as $(K,Na)NbO_3$, $BaTiO_3$ and $Bi_{1/2}Na_{1/2}TiO_3$(BNT)-based ceramics have been widely studied.[1-6)] Among lead-free material systems, $Bi_{1/2}Na_{1/2}TiO_3$(BNT)-based ceramics were found as highly promising lead-free piezoelectric materials due to their relatively high ferroelectric properties. A large piezoelectricity is expected on the BNT-based solid solutions with a composition of morphotropic phase boundary (MPB). To improve the piezoelectric properties of BNT ceramics, some investigators have focused on new BNT-based binary or ternary systems with a morphotropic phase boundary (MPB)[7–15)] Among these systems, the $Bi_{0.5}(Na_{1-x}K_x)_{0.5}TiO_3$ (BNKT) system[8-10)] was reported to exhibit high potential. Sasaki et al.[8)] first reported the MPB between rhombohedral phase (BNT) and tetragonal phase (BKT) to exist in the range of x = 16–20 mol%, where the BNKT ceramics presented good piezoelectric properties. However, a significant problem of BNT-based ceramics is its large leakage current, which results in difficulties to pole the specimens. High leakage current of the BNKT specimens was ascribed to vaporization of Bi during sintering and subsequent defect formation at high temperatures.[16-18)] Vapor pressure of bismuth oxide is higher than that of lead oxide,[19)] implying bismuth oxide in BNT ceramics is easier to vaporize compared with

lead oxide in PZT ceramics. Volatile problems as well as intrinsic point defects usually occur at higher sintering temperatures for BNKT ceramics. However, a suitably high sintering temperature is required to obtain dense microstructures for ceramics. It is therefore believed that competition between vacancy generation and microstructural arrangements after specimen fabrication results in final electrical properties. The sintering behavior in BNKT ceramics is a complicated process. Second phase formation may arise from different thermodynamic stability of elements during sintering, which results in stoichiometric deviation and greatly affects the electrical properties of materials. Although defect behavior is important, few studies had been reported on microstructural characteristics and compositional distribution in BNKT ceramics.

Appropriate element doping can improve dielectric, ferroelectric and piezoelectric properties of ceramics. This is attributed to that additives modify the microstructure, atomic bonds and defect characteristics. According to Ellingham diagram, Li exhibits a lower value of free energy (ΔG^0) than Bi, Na and K during oxidization reaction,[20] implying that Li possesses higher chemical stability. Therefore, Li-doped BNKT ceramics might restrain evaporation of elements and modify the atomic bond.

It has been proposed that crystal growth under very high oxygen pressure is advantageous for suppressing the vacancy formation.[21-24] Vacancy or other defects are closely related to the leakage current and affects polarization switching and poling process in ferroelectric materials. On the other hand, the calculation of reduction energy suggests that the formation of Ti^{3+} and oxygen vacancies under reducing atmospheres (low P_{O2}), which leads to n-type conduction behavior.[25] The migration of oxygen vacancy in $Bi_4Ti_3O_{12}$ ceramics has been estimated by calculation to possess high activation barriers (>1.6 eV), suggesting that high oxygen ion conductivity is unlikely at room temperature.[25] Whether BNKT ceramics contain similar defects or not, need to be clarified in order to reduce the high leakage current of BNKT ceramics after sintering at high temperatures.

Therefore, the purpose of this work is attempted to investigate correlation among defect formation, second phase development during sintering, and their effects on electrical properties for BNKT-based ceramics. At the same time, specimens sintered at different atmospheres, post-oxidization annealing and appropriate Li addition were carried out to understand defect suppression.

2. Experimental Procedures

A conventional solid state reaction technique was adopted to fabricate $(Bi_{0.5}(Na_{1-x}K_x)_{0.5})TiO_3$ (abbreviated as BNKT100x) ceramics with x =0, 0.14, 0.16, 0.18, 0.2, 0.22, 0.8. On the other hand, $(Bi_{0.5}(Na_{0.82-x}K_{0.18}Li_x)_{0.5})TiO_3$ (abbreviated as BNKLTx) ceramics with x = 0, 0.05, 0.075 and 0.1 are also prepared to understand the effect of Li doped in defects and second phase formation. Reagent grade oxides and carbonate powders such as Bi_2O_3, Na_2CO_3, K_2CO_3, Li_2CO_3 and TiO_2 were used as starting raw materials. The powders were ball milled for 24 h and then calcined at

850°C for 2 h. Calcined powders were reground and pressed into disc specimens. The green discs of different compositions were sintered at 1100~1150°C for 2 h in air. BNKT100x ceramics with x = 0.18 were sintered at 1150°C for 2 h in oxygen and nitrogen atmospheres to understand the effect of atmospheres on defect formation. X-ray diffraction (XRD) technique (Max-RC, Rigaku, Japan) was used to determine the crystal phases of the samples. The chemical homogeneity of the specimens was investigated using an energy-dispersive spectrometer (EDS) attached to a transmission electron microscope with a field emission gun (FEG-TEM) (Tecnai G^2 F20) and an FEG scanning electron microscope (FEG-SEM) (JEOL 6500F). Density was measured with Archimedes method using distilled water. The P–E hysteresis loops were obtained by a Sawyer-Tower circuit. Dielectric properties were evaluated using an LCR meter (WK6420C, England) from room temperature to 430℃ with a frequency of 1 kHz. Leakage current was measured using Precision Workstation 2000 (Radiant Technologies, USA) and samples were submerged in a silicone oil bath at room temperatures while DC voltage was applied. Surface chemical compositions and bonding states of the specimens after polish were investigated using an X-ray photoelectron spectroscope (XPS) (VG ESCA Scientific Theta Probe, England).

3. Results and Discussion

The relative densities of the $(Bi_{0.5}(Na_{1-x}K_x)_{0.5})TiO_3$ ceramics at x = 0~0.8 were all higher than 96%. Figure 1(a) shows the X-ray diffraction patterns of BNKT100x specimens sintered with different BKT contents. The patterns of all specimens revealed primarily perovskite structure. However, the XRD diffraction patterns of BNKT100*x* with x = 0.14~0.8 showed a small quantity of potassium titanium oxide $K_2Ti_8O_{17}$ second phase as shown in Fig. 1(b), according to the extra peaks located at the diffraction angles of 11.3°, 12.9° and 29.9°, respectively. Figure 1(b) also shows that the intensities of the peaks corresponding to the second phase become weaker with a decrease of composition x and dropped to zero for the composition with x = 0 (pure BNT ceramics). All powders revealed single perovskite structure after calcinations at 850℃ for 2 h. However, XRD diffraction patterns of sintered specimens show existence of the second phase. According to the study of $B_{0.5}K_{0.5}TO_3$

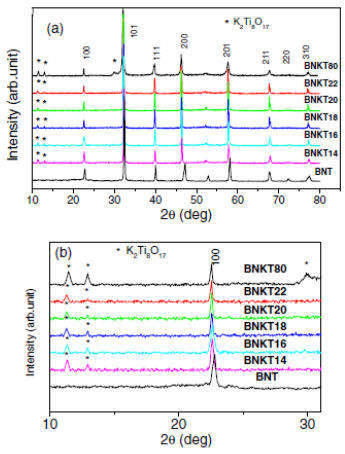

Fig. 1. (Color online) (a) XRD patterns of BNKT100*x* ceramics with different BKT contents and (b) reflections around 2θ of 10–30°.

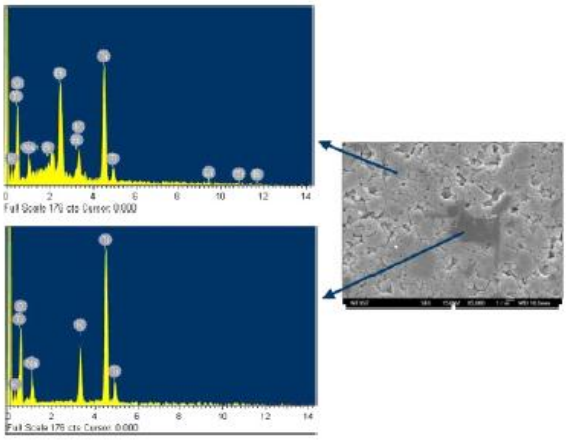

Fig. 2. (Color online) SEM image and EDS spectra of matrix and second phase in BNKT18 specimens sintered at 1150 °C for 2 h in air.

(abbreviated as BKT) ceramics by Takenaka *et al*,[26] the single-phase perovskite structures were observed at sintering temperature lower than 1030°C. However, it was confirmed that second phase peaks ($K_2Ti_6O_{13}$) gradually increased in the sintering temperature range from 1040 to 1060°C, and the sample were then melted at 1070°C. Therefore, second phase formation in BKT ceramics happened in the sintering temperature above 1030 °C. The results show that the second phase simultaneously occurred while the formation of perovskite structure in BKT ceramics at high temperature. Although Takenaka *et al*[26] identified that second phase of $K_2Ti_6O_{13}$ in BKT ceramics is different from the second phase $K_2Ti_8O_{17}$ in the current BNKT ceramics, the reason may be attributed to the difference in K^+ contents between BKT and BNKT ceramics. At the same time, Takenaka et al.[26] proposed that formation of the second phase was attributed to volatilization of the bismuth element. However, we believe that K^+ and Ti^{4+} favoring to form the second phase should be attributed to lower thermodynamic reaction energy during sintering.

In order to clarify the second phase formation mechanism, SEM–EDS were performed to investigate the compositional distribution of the specimens in the matrix and the second phase. The result displays that the second phase exist in a BNKT18 specimen sintered in air as shown in Fig. 2. It is clear that the second phase exhibits darker contrast in the BEI image, and interestingly no Bi was detected in the composition of the phase. To further quantify the variation of composition, TEM–EDS analysis of element revealed compositional distribution of matrix in BNKT18 specimen as shown in Fig. 3 and Table 1. The second phase indeed exists in matrix; meanwhile, Table 1 shows that compositions at different regions of matrix deviate from the stoichiometric composition. The results imply that the formation of $K_2Ti_8O_{17}$ second phase induces a Bi-rich and K-deficient regions in the matrix as shown in Table 1. Meanwhile, the $K_2Ti_8O_{17}$ second phase exhibits Bi-free and K-rich composition. Although Bi is an element showing high volatility, evaporation leading to the Bi-free second phase and Bi-rich matrix is unlikely. We also note that the calcined BNKT powders exhibit a simple perovskite structure. The results indicate that the second phase formation was attributed to thermodynamic stability of potassium titanate rather than simply Bi-evaporation.

Extra Bi was expelled to grain interior, which induce high content Bi in the matrix. In order to understand compositional difference within grains and grain boundaries, we also use TEM-EDS analysis to examine the samples, as shown in Table 1. The results show very limited composition difference between grains and

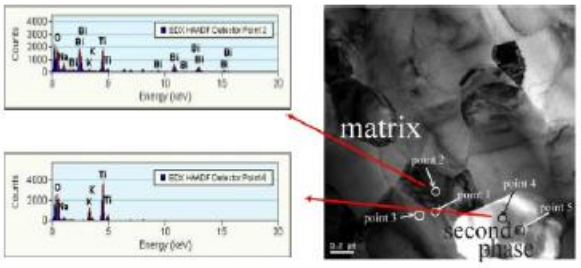

Fig. 3. (Color online) TEM image and EDS spectra of matrix and second phase in BNKT18 specimens sintered at 1150 °C for 2 h in air.

Table I. TEM–EDS compositional analysis of matrix and second phase in BNKT18 specimens sintered at 1150 °C for 2 h in air (unit: at. %).

	Element				
	Bi	Na	K	Ti	O
Point 1 (boundary)	18	8	0.8	22	52
Point 2 (grain)	17	8	0.3	23	51
Point 3 (grain)	20	7	1.4	24	48
Average value	18	8	0.8	23	50
Stoichiometry	10	8	1.8	20	60
Point 4 (impurity)	0	1.6	6.1	31	61
Point 5 (impurity)	0	1.5	6.9	32	59

Table II. Comparisons of XPS parameters of Ti ion for the BNKT18 ceramics sintered at 1150 °C for 2 h in (a) oxygen, (b) air, and (c) nitrogen atmospheres.

Treatment condition	Element/ ion state	Core level	Binding energy (eV)	FWMH (eV)	ΔeV[a)]	Area of subpeak	Area sum	Area (%)
(a)	Ti^{4+}	$2p_{3/2}$	457.20	1.3	6	—	—	100
		$2p_{1/2}$	463.20	2.4		—		
	Ti^{3+}	$2p_{3/2}$	—	—	—	—	—	0
		$2p_{1/2}$	—	—		—		
(b)	Ti^{4+}	$2p_{3/2}$	457.60	1.3	5.5	422	901	81
		$2p_{1/2}$	463.10	2.4		479		
	Ti^{3+}	$2p_{3/2}$	456.10	1	5.7	50	211	19
		$2p_{1/2}$	461.80	2.1		161		
(c)	Ti^{4+}	$2p_{3/2}$	457.60	1.3	5.65	391	852	71.7
		$2p_{1/2}$	463.25	2.4		461		
	Ti^{3+}	$2p_{3/2}$	456.05	1	5.5	125	336	28.3
		$2p_{1/2}$	461.55	2.1		211		

a) ΔeV denotes spin–orbit splitting of element.

grain boundaries, which indicated no obvious segregation of elements at the grain boundaries. Fracture surface investigations by SEM displayed transgranular fracture which implies that strength of grain boundaries is higher than that of grains.

In addition to meso-scale microstructures, such as the second phase mentioned above, atomic scale and finer defects were also examined. BNKT ceramics sintered under different atmospheres and post annealing treatments were carried out and X-ray photoelectron spectroscopy (XPS) technique was used to characterize defect formation. Figure 4 shows the narrow-scan XPS spectra of Ti in BNKT18 ceramics sintered in air, oxygen atmosphere (higher P_{O2}) and nitrogen atmosphere (lower P_{O2}), respectively. These experimental curves were fitted by symmetrical Gaussian-Lorentzian function after background subtraction. Intriguingly, it could be observed that Ti^{3+} and Ti^{4+} coexist in BNKT18 ceramics sintered in air. The binding energy of Ti ($2p_{3/2}$) and Ti ($2p_{1/2}$) peaks corresponding to Ti^{3+} are 456.1 and 461.8eV, whereas peaks corresponding to Ti^{4+} are 457.6 and 463.1eV. The results indicated Ti valence transition. The same results were also observed in the specimens sintered in nitrogen atmospheres and showed larger amount of Ti^{3+}. According to the fitting results shown in Table 2, the amount of Ti^{3+} is the maximum (28.3 at%) in nitrogen atmosphere (lower P_{O2}), which implied that the reduced atmosphere easily transforms Ti^{4+} ion to Ti^{3+} ion. According to calculations by Snedden *et al.* for $Bi_4Ti_3O_{12}$,[25] the reduction process involving Ti^{3+} and oxygen vacancy formation is energetically favorable. It is therefore predicted that $Bi_4Ti_3O_{12}$ may form oxygen vacancies, simultaneously accompanied with Ti valence transition (Ti^{4+} to Ti^{3+}). Since Ti^{4+} is rather easily reduced to Ti^{3+} by placement of an electron in the empty 3d conduction band levels. The results produce shallow donor

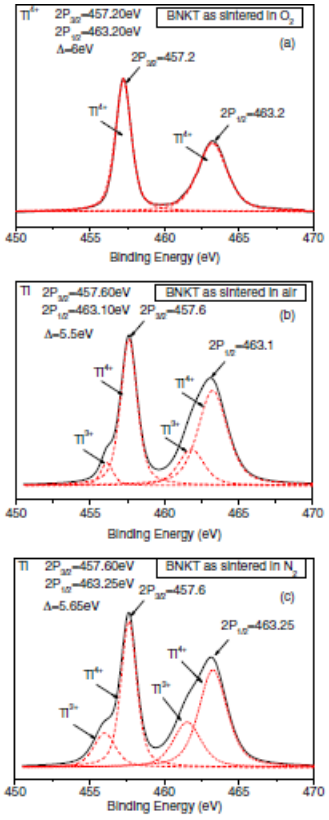

Fig. 4. (Color online) XPS spectra of Ti ion in BNKT18 ceramics sintered at 1150 °C for 2 h in (a) O_2, (b) air, and (c) N_2. The spectra of specimens sintered in nitrogen and air atmosphere show Ti^{4+} and Ti^{3+} ion states and those of specimens sintered under higher P_{O2} (oxygen atmosphere) show only Ti^{4+} ion states.

levels of Ti.[27] Thus, lower oxygen atmosphere induces more oxygen vacancies and Ti valence transition (Ti'_{Ti}). The reaction can be described as following：

$O_O^* \rightarrow V_O^{\cdot\cdot} + 2e' + 1/2\ O_2\,(g)$**……. (1)**

$Ti_{Ti}^* + e' \rightarrow Ti'_{Ti}$**……. (2)**

$O_O^* + Ti_{Ti}^* \rightarrow V_O^{\cdot\cdot} + Ti'_{Ti} + 1/2\ O_2\,(g) + e'$**……. (3)**

Where Ti_{Ti}^* denotes Ti^{4+} at the Ti site, O_O^* denotes oxide ion at the oxygen site, Ti'_{Ti} denotes Ti^{3+} at the Ti site and $V_O^{\cdot\cdot}$ denote oxygen vacancy.

Because easily volatile elements such as bismuth, sodium and potassium exist in BNKT ceramics, defects are easily produced during sintering. According to the study of $Bi_4Ti_3O_{12}$ by Noguchi *et al,*[28] V_{Bi}''' is easily generated at high temperatures accompanied with the nearest-neighbor $V_O^{\cdot\cdot}$ to maintain charge balance during defect formation, while bismuth escapes from lattice position and evaporate as Bi_2O_3(g). Formation of oxygen vacancies arises from evaporation of Bi and lower oxygen atmosphere, which is accompanied with the Ti valence transition to maintain charge balance during defect formation. Therefore, the whole reaction can be described again as follows：

$4\ Bi_{Bi}^* + 7O_O^* + Ti_{Ti}^* \rightarrow 4V_{Bi}''' + 6V_O^{\cdot\cdot} + Ti'_{Ti} + 1/2O_2\,(g) + e'$**……. (4)**

Ti valence transition (Ti'_{Ti}) results in electron hopping mechanism, which might play an important role in leakage current behavior in the present material system at room temperatures.

Figure 4 also showed XPS spectra of Ti ion in the BNKT18 ceramics under oxygen atmosphere (higher P_{O2}). The spectra indicated that the Ti $2p_{3/2}$ and $2p_{1/2}$ states contain only the contributions from Ti^{4+} ion states. Therefore, Ti valence transition (Ti^{4+} to Ti^{3+}) is absent as shown in Table 2. On the other hand, post annealing treatments were carried out for BNKT18 ceramics sintered in air. Fig. 5(a) shows the XPS spectra of Ti for BNKT18 ceramics annealed in air at 800℃ for 4h, indicating that Ti^{3+} content decreases in BNKT18 ceramics. After annealing treatment at 1000℃ for 4h, the Ti^{3+} content is absent as shown in Fig. 5(b). The result implies that thermal annealing in oxygen atmosphere reduces Ti^{3+} ion states and might be expressed the following reaction：

$V_O^{\cdot\cdot} + 1/2\ O_2 + 2Ti'_{Ti} \rightarrow O_O^* + 2\ Ti_{Ti}^*$ **……. (5)**

Due to oxidization treatment, the oxygen in air enters the $V_O^{\cdot\cdot}$ and leads Ti^{3+} ion state to transform to Ti^{4+} ion state to maintain charge balance. This might result in less oxygen vacancies and electron hopping due to Ti valence transition. Therefore, sintering under higher oxygen atmosphere and post annealing treatment are advantageous approaches and could effectively reduce defects of Ti valence transition and oxygen vacancies.

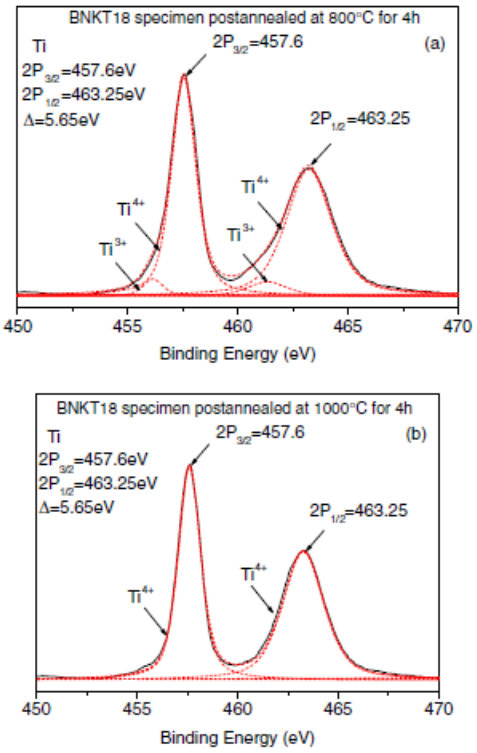

Fig. 5. (Color online) XPS spectra of Ti ion in BNKT18 ceramics (a) post-annealed in air at 800 °C for 4 h, indicating Ti^{3+} content decrease and (b) post-annealed in air at 1000 °C for 4 h showing Ti^{3+} content is absent.

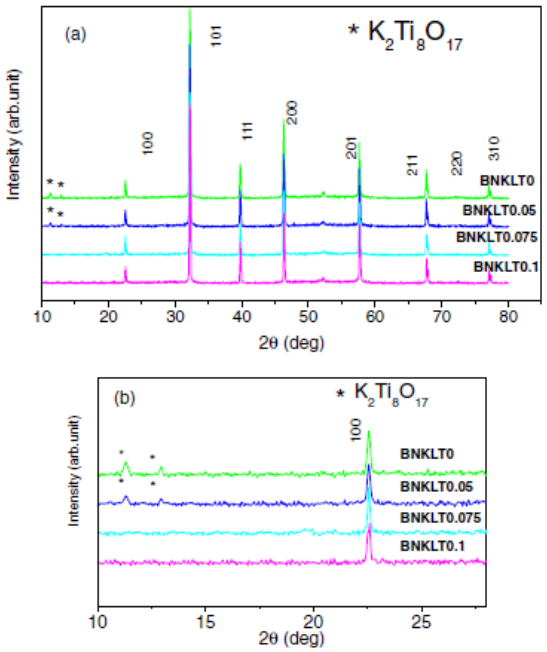

Fig. 6. (Color online) (a) XRD of BNKLT*x* ceramics with different Li contents at $x = 0$, 0.05, 0.075, and 0.1 and (b) reflections around 2θ of 10–30°.

Table III. SEM–EDS compositional analysis of (a) BNKT18 ceramics sintered at 1150 °C for 2 h in O_2 and (b) BNKLT0.075 ceramics sintered at 1150 °C for 2 h in air (unit: at. %).

(a)	Bi	Na	K	Ti	O
Actual value	15	7.6	1.3	22	58
Stoichiometry	10	8.2	1.8	20	60
(b)	Bi	Na	K	Ti	O
Actual value	12	7.9	1.7	21	55
Stoichiometry	10	7.5	1.8	20	60

It was reported that high leakage current of BNKT ceramics was attributed to defects produced by evaporation of Bi_2O_3.[16-18] However, we have demonstrated that second phase, $K_2Ti_8O_{17}$, appears during processing due to thermodynamic stability of the phase. It can be expected that K and Ti were extracted out from the original perovskite lattice, when the second phase forms. However, the remained Bi, Na, K and O construct a defective perovskite with many oxygen and Ti vacancies. This may induce an oxygen-deficient and reducing environment in the material, which contribute to Ti valence transition and therefore high leakage current for BNKT materials.

According to our previous work,[29] Li doped BNKT ceramics exhibit higher density and electrical properties than pure BNKT ceramics. In order to get a better understanding on effect of doping elements, further analysis were examined in Li doped BNKT18 ceramics. X-ray diffraction patterns of BNKLT specimens sintered in air with x = 0, 0.05, 0.075 and 0.1 were revealed in Fig. 6(a). The crystal structures of Li-doped BNKT materials also exhibited well-defined perovskite structure. However, second phase became weaker with increase of x; second phase were not found while x = 0.075 and 0.1 as shown in Fig. 6(b). The result indicated that Li doped BNKT ceramics suppress second phase formation. Ionic radius of Li^+ is smaller than that of Na^+ and K^+ and partial substitution of A-site ions by Li^+ decreases the lattice distortion, which reduces internal stress and makes the dipoles easier to switch and

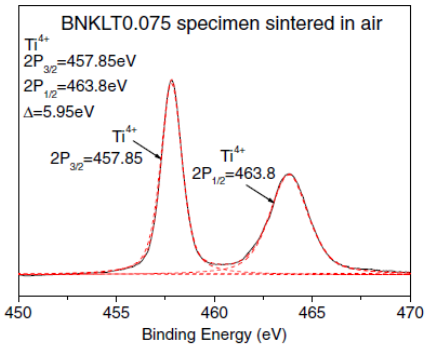

Fig. 7. (Color online) XPS spectra of Ti ion showing only Ti^{4+} ion states in BNKLT0.075 specimen sintered at 1150 °C for 2 h in air.

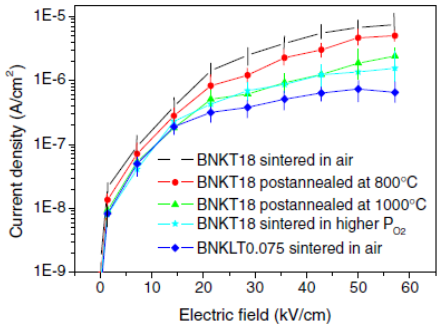

Fig. 8. (Color online) Leakage current density (*J*) as a function of electric field (*E*) in BNKT18 ceramics sintered under different atmospheres.

promote the domain orientation. However, excessive addition might generate instability of structure and poor electrical properties. Our results indicate that Li doped BNKT ceramics with x=0.075 exhibit the highest ferroelectric and piezoelectric properties than the other contents of Li. Therefore, SEM-EDS were performed to investigate the compositional characteristics of the BNKLT0.075 specimens. SEM–EDS semi-quantitative results revealed composition distribution of matrix in BNKLT0.075 specimen as shown in Table 3. Compared with BNKT18 specimen, BNKLT0.075 specimen exhibited less compositional inhomogeneity. X-ray diffraction patterns of BNKLT0.075 specimens did not exhibit the second phase, showing better homogeneity of composition. On the other hand, XPS was carried out to evaluate the characteristics of Li doping in the material. Figure 7 shows the XPS spectra of Ti in BNKLT0.075 ceramics sintered at 1150^{o}C for 2 h in air, which indicates only Ti^{4+} ion state. The binding energies of $2p_{3/2}$ and $2p_{1/2}$ peaks corresponding to Ti^{4+} are 457.85 and 463.8eV. The doublet peaks were observed slightly shifting toward higher binding energy than that of BNKT18 ceramics. This result indicates stronger bond from A, B-site cations and oxygen to stabilize the structure. In fact, BNKLT0.075 ceramics with tolerance factor t = 0.990, which is close to unity and suggests a relatively stable perovskite structure. Therefore, Li addition has an effect on strengthening the bonding of the perovskite structure. This will restrict second phase formation and Ti valence transition. This might result in Li doped BNKT ceramics exhibit higher insulating, ferroelectric, dielectric and piezoelectric properties.

Leakage current, ferroelectric and dielectric measurements were carried out to understand the effects of defects on electrical properties. To clarify the correlation between leakage current and defects in BNKT ceramics, the leakage current density (*J*) as a function of electric field (*E*) was measured at room temperature as shown in Fig.8, which shows that BNKT18 ceramics sintered in air exhibiting higher leakage current density (*J*) over 10^{-6} A/cm^2. The high leakage current might be attributed to electrons hopping from Ti^{4+} to Ti^{3+} state. BNKT18 ceramics annealed at 800 ℃ for 4 h in air displayed a decrease in leakage current. The ceramics annealed at 1000 ℃ for 4h in air revealed an even lower value of leakage current, which is due to an increase of Ti valence ($Ti^{3+} \rightarrow Ti^{4+}$) and smaller amount of n-type conduction as expressed by Eq. (5). It can be seen that annealing processes under the same electric fields exhibit

lower leakage current density (J) values than as-sintered BNKT18 ceramics. On the other hand, BNKT18 ceramics as-sintered in O_2 atmosphere display a decrease in leakage current, which resulted from oxidation treatment inhibiting formation of oxygen vacancies and Ti valence transition. The leakage current measurements of Li doping were also carried out. The BNKLT 0.075 ceramics sintered in air reveal a relatively lower leakage current. The result is attributed to Li doping strengthening bonding energy and results in the reduction in the oxygen vacancies and Ti valence transition. Compared with above results, Li doping ceramics display the lowest leakage current. Ceramics as-sintered in higher oxygen atmosphere and post-annealing treatment processes can decrease leakage current and promote insulating properties in materials.

Figure 9 shows that polarization hysteresis loops of BNKT18 specimens sintered in air, O_2 and BNKLT0.075 specimens sintered in air. The values of the remanent polarization and coercive field are 33.4 C/cm^2, 40.5kV/cm, respectively for BNKT18 samples sintered in air and 35.9 C/cm^2, 37.9kV/cm for the BNKLT0.075. However, BNKT18 samples sintered in O_2 indicate that the highest value of P_r is 38.4 C/cm^2 and the lowest value of coercive field E_c is 36.2kV/cm. The enhancement of ferroelectric properties may be associated with the fact of less oxygen vacancies in BNKT18 samples sintered in O_2. In general, treatments of specimens in higher oxygen atmosphere inhibit the generation of oxygen vacancies. It has been known that oxygen vacancy is one of the main reason of reducing the domain-wall motion.[30-31] The smaller amount of oxygen vacancies enhances the switchability of polarization and becomes easier switching in polarization vectors under the applied electric field. From compositional analysis of SEM-EDS as shown in Table 3, chemical stoichiometry of oxygen element in BNKT18 samples sintered in O_2 revealed the least oxygen-deficiency and thus promotes ferroelectric properties. Figure 10 shows temperature dependence on dielectric constant at 1 kHz frequency for BNKT18 specimens sintered in air, O_2 and BNKLT0.075 specimens sintered in air. The dielectric constant (ε_r) of the BNKLT0.075 specimen sintered in air displays a maximum value. The addition of Li to BNKT ceramics promotes dielectric constant, which might be attributed to the reduction in the number of Ti valence transition and oxygen vacancies. The result promotes insulating properties in materials and therefore increases dielectric constant.

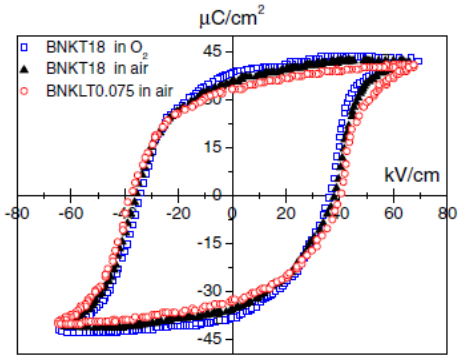

Fig. 9. (Color online) Polarization hysteresis loop in BNKT18 ceramics sintered in air, O_2, and Li-doped specimens sintered in air.

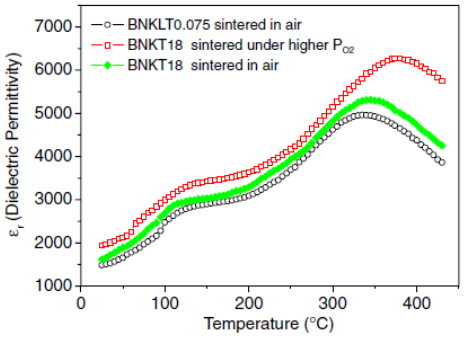

Fig. 10. (Color online) Temperature dependence of dielectric constant at 1 kHz frequency for BNKT18 specimens sintered in air, O_2 and Li-doped specimens sintered in air.

4. Conclusions

Second phase formation in BNKT ceramics might arise from thermodynamic stability of potassium titanate during sintering. The results produce compositional inhomogeneity and generate more oxygen and titanium vacancies in defective perovskite lattice, which obviously affects electrical properties in BNKT ceramics. The specimens sintered under higher oxygen atmosphere and post-oxidation annealing treatment could improve Ti valence transition and effectively decreases the leakage current. On the other hand, Li addition to BNKT ceramics can suppress formation of second phase and Ti valence transition, which decreased leakage current and promoted ferroelectric and dielectric properties. This might be attributed to that Li addition contributes to the binding energy among A, B-site cations with oxygen to stabilize the structure.

Acknowledgements

Authors are thankful to National Science Council of Taiwan for financial support under the project No: 97-2923-M-029-001-MY3.

References

1) Y. Saito, H. Takao, T. Tani, T. Nonoyama, K. Takatori, T. Homma, T. Nagaya, and M. Nakamura: Nature **432** (2004) 84.
2) E. Hollenstein, M. Davis, D. Damjanovic, and N. Setter: Appl. Phys. Lett. **87 (**2005) 182905.
3) H. Birol, D. Damjanovic, and N. Setter: J. Am. Ceram. Soc. **88 (**2005) 1754.
4) T. Karaki, K. Yan, T. Miyamoto, and M. Adachi: Jpn. J. Appl. Phys. **46** (2007) L97.
5) X. X. Wang, X. G. Tang, and H. L. W. Chan: Appl. Phys. Lett. **85** (2004) 91.
6) D. Lin, D. Xiao, J. Zhu, and P. Yu: Appl. Phys. Lett. **88** (2006) 062901.
7) T. Takenaka, K. Maruyama, and K. Sakata: Jpn. J. Appl. Phys. **30** (1991) 2236.
8) A. Sasaki, T. Chiba, Y. Mamiya, and E. Otsuki: Jpn. J. Appl. Phys. **38** (1999) 5564.
9) J. Kreisel, and A. M. Glazer: J. Phys. Condens. Matter. **12** (2000) 9689.
10) G. O. Jones, J. Kreisel, and P. A. Thomas: Powder Diffr. **17** (2002) 301.
11) H. Ishii, H. Nagata, and T. Takenaka: Jpn. J. Appl. Phys. **40** (2001) 5660.
12) B. J. Chu, D. R. Chen, G. R. Li, and Q. R. Yin: J. Eur. Ceram. Soc. **22 (**2002) 2115.
13) H. Nagata, M. Toshiba, Y. Makiuchi, and T. Takenaka: Jpn. J. Appl. Phys. **42 (**2003) 7401.
14) X. X. Wang, X. G.Tang, and H. L. W. Chan: Appl. Phys. Lett. **85 (**2004) 91.
15) D. Q. Xiao, D. M. Lin, J. G. Zhu, and P. Yu: J. Electroceram. **16 (**2006) 271.
16) R. Zuo, S. Su, Y. Wu, J. Fu, M. Wang, and L. Li: Mater. Chem. Phys. **110** (2008) 311.
17) R. Zhang, J. F. Li, B. P. Zhang, and C. E. Peng: J. Appl. Phys. **103** (2008) 074109.
18) X. Wang, X. G. Tang, K. W. Kwok, H. L. W. Chan, and C. L. Choy: Appl. Phys.

A: Mater. Sci. Process. **80** (2005) 1071.
19) Y. Wu, and G. Cao: Appl. Phys. Lett. **75** (1999) 2650.
20) D. R. Gaskell: *Introduction to the thermodynamics of materials* (Taylor & Francis, New York, 2003) p. 337.
21) Y. Noguchi, T. Matsumoto, and M. Miyayama: Jpn. J. Appl. Phys. **44** (2005) L570.
22) M. Takahashi, Y. Noguchi, and M. Miyayama: Jpn. J. Appl. Phys. **41** (2002) 7053.
23) Y. Kizaki, Y. Noguchi, and M. Miyayama: Appl. Phys. Lett. **89** (2006) 142910.
24) Y. Noguchi, M. Soga, M. Takahashi, and M. Miyayama: Jpn. J. Appl. Phys. **44** (2005) 6998.
25) A. Snedden, P. Lightfoot, T. Dinges, and M. S. Islam: J. Solid State Chem. **177** (2004) 3660.
26) Y. Hiruma, R. Aoyagi, H. Nagata, and T. Takenaka: Jpn. J. Appl. Phys. **44** (2005) 5040.
27) D. M. Smyth: Solid State Ionics. **129** (2000) 5.
28) T. Goto, Y. Noguchi, M. Soga, and M. Miyayama: Mater. Res. Bull. **40** (2005) 1044.
29) P. Y. Chen, C. C. Chou, T. Y. Tseng, and Haydn Chen: Ferroelectrics **381** (2009) 100.
30) S. E. Park, and S. J. Chung: J. Am. Ceram. Soc. **79** (1996) 1290.
31) U. Robels, L. Schneider, and G. Arlt: Ferroelectrics **133** (1992) 223.